In Situ Magnetohydrodynamic Energy Generation for Planetary Entry Systems

AE8900 MS Special Problems Report
Space Systems Design Lab (SSDL)
Guggenheim School of Aerospace Engineering
Georgia Institute of Technology
Atlanta, GA

Author:
Hisham K. Ali

Advisor:
Dr. Robert D. Braun

May 1, 2015

In Situ Magnetohydrodynamic Energy Generation for Planetary Entry Systems

Hisham K. Ali [*] and Robert D. Braun[†]
Space Systems Design Laboratory, Georgia Institute of Technology
270 Ferst Drive, Atlanta, GA 30331

Proposed missions such as a Mars sample return mission and a human mission to Mars require landed payload masses in excess of any previous Mars mission. Whether human or robotic, these missions present numerous engineering challenges due to their increased mass and complexity. To overcome these challenges, new technologies must be developed, and existing technologies advanced. Mass reducing technologies are particularly critical in this effort. The proposed work aims to study the suitability of various entry trajectories for reclaiming vehicle kinetic energy through magnetohydrodynamic energy generation from the high temperature entry plasma. Potential mission and power storage configurations are explored, with results including recommended trajectories, amount of kinetic energy reclaimed, and additional system mass for various energy storage technologies.

Nomenclature

A	=	vehicle characteristic area
A_c	=	generator area
B	=	magnetic field strength
C_D	=	drag coefficient
L_i	=	generator interaction length
m	=	vehicle mass
n_e	=	electron number density
$\bar{r}$	=	radial distance between vehicle and Mars center of mass
u	=	vehicle velocity
β	=	ballistic coefficient
μ_{Mars}	=	mars gravitational parameter
ρ	=	atmospheric density

[*] Graduate Research Assistant, Aerospace Engineering
[†] David and Andrew Lewis Professor of Space Technology, Aerospace Engineering

I. Introduction and Motivation

FUTURE missions to Mars such as a Mars sample return mission and potential human mission will require much higher masses than have ever been landed on Mars. Previous Mars missions have relied primarily on Viking era technology for entry descent and landing.[1] The limit of this technology is being reached, with the Mars Science Laboratory (MSL) landing system in 2012 illustrating the difficulty in high mass Martian landings.

To achieve humanity's goals for Mars exploration, significant technology development is required. Mass reducing technologies are particularly critical in this effort. Not only does a larger mass require more fuel to launch, but it also carries significantly more kinetic energy that must be reduced to near zero if the vehicle is to land safely. Previous Mars missions have shown that the majority of the vehicle's kinetic energy is dissipated during the hypersonic phase, about 92.5% in the case of Mars Pathfinder.[2] During this hypersonic phase of entry, there exists a highly heated, ionized flow around the vehicle. The free electrons in the flow can be potentially harnessed to create a sustained, usable electric current via magnetohydrodynamic (MHD) power generation, reclaiming some of the vehicle's dissipated kinetic energy.

MHD vehicle interaction for high speed aerospace applications has been studied since the dawn of the space race, with early theoretical studies dating back to the fifties and early sixties.[3] These studies focused primarily on the flow control applications possible with MHD interaction for purposes such as drag and peak heating modulation. At the time, such studies were limited by available technologies, as the magnetic coils needed to produce the necessary magnetic field were mass prohibitive. Since that time, however, dramatic advances in energy storage and magnetic field generation have been made, and in conjunction with a pressing need to reduce interplanetary launch masses, warrants additional investigation of the topic.

Previous research indicates that MHD energy generation can be a useful part of future Mars missions.[4] MHD energy generation is supported by physics, and numerous energy generation schemes have been proposed and studied.[5] Preliminary analysis based on an entry trajectory similar to the Mars Pathfinder Mission suggests that 100MJ per square meter of electrode area could be generated.[6] However, strong magnetic fields on the order of 1T are required, as well as power equipment to store and handle the generated energy.

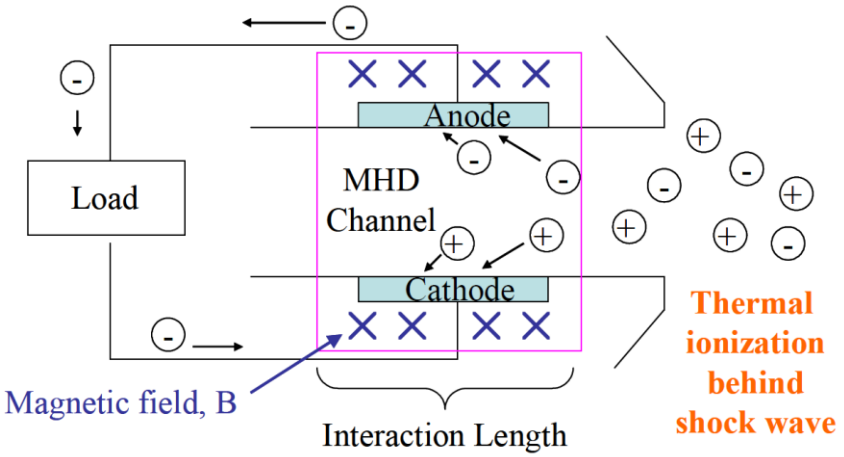

Figure 1. MHD energy generator schematic

A potential MHD generator system for an entry application consists of the following elements: modular MHD generator matrix, electrical current distribution unit, electrical energy storage system, active thermal shield cooling and entry black out mitigation, subsystem for active cooling of temperature sensitive components, resistive load network for heat distribution, oxygen harvesting and separation unit, and rigid, thermo-resistant inflatable containers for oxygen or carbon dioxide storage.[7] Together, these elements create the capability to simultaneously reduce heat shield thermal protection system requirements, reduce entry signal blackout, compress and store atmospheric carbon

dioxide, generate oxygen for later use on the surface, and of course obtain and store power for subsequent use during later stages of entry, descent, and landing or on the surface.

For a conventional internal MHD generator, the amount of power that can be extracted is linear with ambient electron number density and quadratic with flow velocity in the flow regimes of interest for planetary entry.[4] Thus, for a given MHD generator configuration, increased velocity and electron number density will increase output power. The ambient electron number density is driven by ionizing reactions taking place in the high temperature post shock region, and for a traditional direct entry trajectory is significant for a relatively short period of time. For example, the aforementioned 92.5% of kinetic energy lost during the hypersonic phase occurs in less than 60s, presenting difficulties in implementing an energy storage system capable of handling the load. It is estimated that for a Mars Pathfinder type space craft, about 14MJ of energy per m^2 of electrode area can be reclaimed during this period; however, this energy generation occurs over about 30s at a rate of nearly 1 MW.[4] If the energy storage device cannot accept power at this rate, then much of the energy will go to waste. Unfortunately, the ability of an energy storage device to accept energy at a high rate is coupled to its mass, making claiming all of the available energy through a potential challenge.[8]

One proposed alternative is to employ a multi-pass trajectory framework to increase the time spent in the atmosphere and harvest energy at a more manageable rate.[4] The challenge of this approach lies in maintaining enough velocity to cause the atmosphere to ionize in order to raise the electron number density to suitable levels. Additional challenges include the fact that the entry velocity must be sufficiently low to enable exit from the atmosphere on an elliptic orbit while also having a non-zero flight path angle. This challenge is primarily navigational, based on the initial flight path angle.

It was found that seeding the post shock flow region with small amounts of alkali metals such as potassium or cesium dramatically increases electron number density at concentrations up to 1% owing to their comparatively lower ionization energies.[5] Seeding the flow while employing multi-pass trajectories would allow for sustained power generation for multiple orders of magnitude more time, potentially increasing the amount of energy that can be stored with conventional electrical energy storage technologies.

The concept of aerobraking for interplanetary missions has been studied for quite some time, with most initial focus on Mars and Venus.[9] Aerobraking has primarily been utilized for science payloads to assist in transferring the satellite from its hyperbolic interplanetary trajectory to its intended orbit around the target body. Typically, aerobreaking campaigns begin with propulsive orbit insertion to place the spacecraft on an elliptic trajectory with respect to the planetary body, followed by multiple controlled passes and a propulsive burn to achieve the final desired orbit. Notable missions to Mars that have employed aerobraking include the 1997 Mars Global Surveyor[10], 2001 Mars Odyssey[11], and 2006 Mars Reconnaissance Orbiter[12]. These aerobraking maneuvers lasted for significant amounts of time, with the maneuvers taking four and a half months, three months, and five months respectively.

Aerobraking operations that have been studied for MHD power generation take place during significantly shorter periods of time on the order of hours. Previous work studied multi-pass entry, descent, and landing trajectories, termed E^iDL, where *i* represents the number of atmospheric passes. These orbit cases were generated by assuming an entry velocity and vehicle mass and varying the system drag area.[4]

In the above case, varying the drag area produced 3, 7, and 11 pass entry paths spending 1881s, 4390s, and 7400s in the atmosphere respectively. The analysis was carried out for a 1000kg sample entry vehicle with a drag coefficient of 0.4, yielding an average of 500MJ per square meter of electrode area per pass. It is also claimed that future carbon nanotube based superconducting energy storage devices could store this energy with approximately 200 kg of added system mass, but without this technology, the additional mass requirement would become approximately 3000kg.[4]

It would be of great benefit to extend this analysis to various types of entry vehicles, and also to attempt to control the number of atmospheric passes through only the initial position and velocity states at the Mars atmospheric boundary. The proposed trajectories would consist of an aerocapture pass in which the space craft is transferred from a hyperbolic interplanetary trajectory followed by a brief aerobraking campaign and concluding with entry from orbit. Furthermore, advances in electrical energy storage technologies since the publication of previous results warrants additional review. The contributions contained herein are an effort to achieve these goals. They consist of a multi-pass trajectory simulator, a post-shock electron number density model, a MHD energy generation power availability model, and an

electrical energy storage system performance model applied to various trajectories, vehicle configurations, and energy storage technologies. Results presented include total amount of energy available for storage, mass estimates for storing all available energy with various electrical energy storage systems, and minimum electrical energy storage system performance required to store all available energy within a given mass constraint.

II. Relevant Background and Theoretical Approach

A. Determining the Power Available for MHD Energy Generation

The total energy available via MHD energy generation is the integration of the power available for a MHD generator along a given trajectory. To actually calculate this power generation profile, it is necessary to identify the relevant physical interactions occurring along a given trajectory. These interactions are the gravitational interaction between planetary body and spacecraft, the aerodynamic interaction between planetary atmosphere and spacecraft, and the thermochemical interaction within the atmosphere as the spacecraft moves at hypersonic speed. The superimposed effects of these three physical interactions allow for the definition of the position state, velocity state, and electron number density. These states define the total power that can be generated by MHD energy conversion. For a conventional internal MHD generator, the generated power behaves the following scaling law[4]

$$\boldsymbol{P \propto n_e u^2 B^2 A_c L_i} \tag{1}$$

Where P is the generator power output, n_e is the ambient electron number density, u is the flow velocity, B is the magnetic field strength, A_c is the generator area, and L_i is the generator length. For the purposes of this analysis, the magnetic field strength will be assumed in all cases to be a constant 0.2 Tesla. The generator area will be assumed to be 1 square meter in all cases as well, with a characteristic length of 1 meter. As a result, the above scaling law can be reduced to a function of electron number density and velocity only.

The velocity can be calculated by defining the system dynamics and integrating to obtain position and velocity. Taking into account the gravitational and aerodynamic interaction, the Equation of motion shown as equation 2 below for the system relative to the Martian center of mass is solved.

$$\ddot{\bar{r}} = -\frac{\boldsymbol{\mu_{Mars}}}{(\bar{r}\cdot\bar{r})^{3/2}}\bar{r} - \frac{\boldsymbol{\rho}(\dot{\bar{r}}\cdot\dot{\bar{r}})}{\boldsymbol{2\beta}}\hat{\dot{\bar{r}}} \tag{2}$$

where β is the ballistic coefficient of the entry vehicle, a similarity parameter that governs the hypersonic flight, defined below as follows:

$$\boldsymbol{\beta = \frac{m}{C_D A}} \tag{3}$$

where m is the entry vehicle mass, C_D is the entry vehicle drag coefficient, and A is the entry vehicle area.

To calculate the electron number density, the atmospheric properties and composition after passing through a shock wave must be calculated. Since the ambient density, pressure, and temperature can be calculated as functions of altitude, and Martian atmospheric species composition is known and assumed to be constant, the addition of velocity fully specifies the post shock state. A chemical equilibrium solver, in this case NASA's Chemical Equilibrium and Applications (CEA) code, is then used to calculate the post shock state.[13]

Table 1 Martian Atmospheric Compositions[14]

Constituent	Relative Abundance
CO_2	96.0%
Ar	1.9%
N_2	1.9%
O_2	0.14%
CO	0.06%

Martian atmospheric constituents and their abundances are presented above as table 1 in order of relative abundance.[14] Post shock species include: Ar, C, N, O, C_2, N_2, O_2, CN, CO, NO, CO_2, NCO, Ar^+, C^+, C_2^+, N^+, N_2^+, O^+, O_2^+, CN^+, CO^+, NO^+, and e^-. In the case of seeding, there will also be K+ present in the post-shock species. Using these data in

conjunction with the atmospheric properties as a function of altitude, the post shock temperature, pressure, and species composition can be calculated as a function of velocity.

Once the species composition, temperature, and pressure are known, the equilibrium electron number density is calculated using the post shock density, molecular weight, and electron mole fraction. Equilibrium electron number density is strongly dependent on the post shock temperature, and the standard Mars atmospheric constituents fail to yield sufficient electron number density for MHD energy generation below velocities of 5 km/s. However, previous work indicates that seeding the post-shock flow with a small amount of easily ionizable species such as alkali metals can boost the electron number density. This seeding could be accomplished with nozzles near the stagnation region or by impregnating the seed material into the TPS.[4] For example seeding the flow in the vicinity of the MHD Generator with 1% potassium by mass results in multiple order of magnitude increases in electron number density.[5] Results for unseeded and 1% potassium seeded electron number density as a function of vehicle velocity and altitude are presented below as Figures 2 and 3. Figure 4 illustrates the post shock electron number density vs velocity at 0 and 100km altitude for a variety of potassium seeding levels up to 1%.

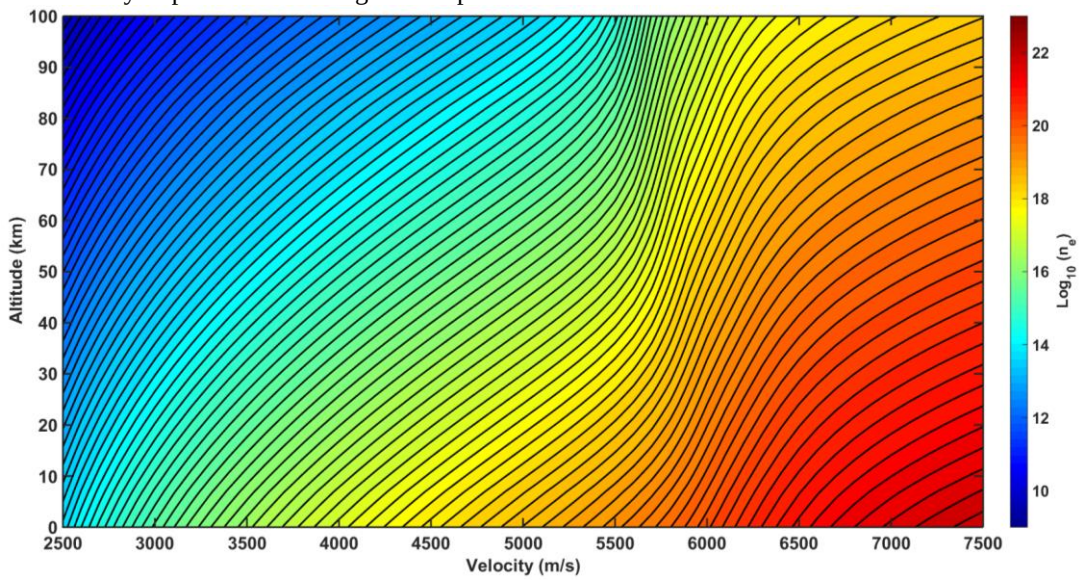

Figure 2. 0% K Seeded electron number density (#/m^3) as a function of Mars altitude and vehicle velocity.

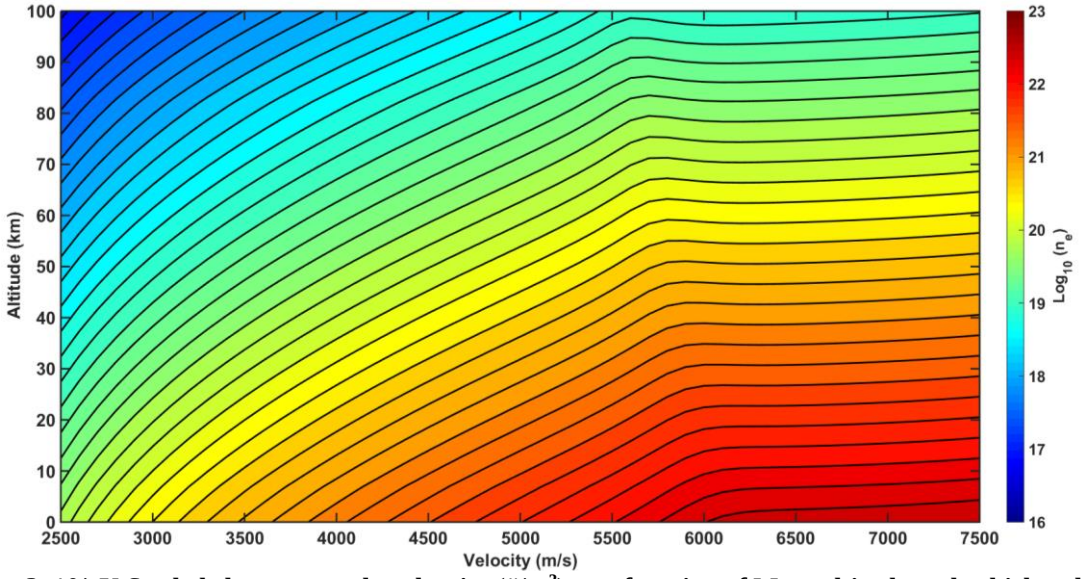

Figure 3. 1% K Seeded electron number density (#/m^3) as a function of Mars altitude and vehicle velocity.

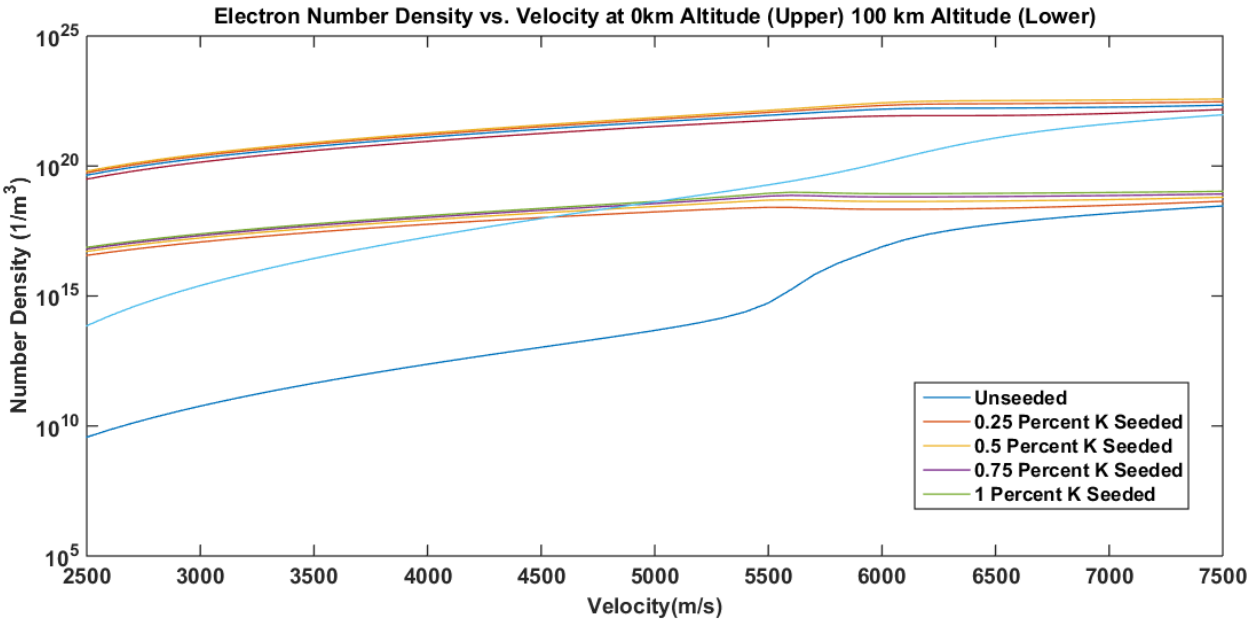

Figure 4. Electron Number density vs. velocity at 0 km altitude (upper) and 100 km altitude (lower).

After the numerical integration has been done to calculate the trajectory and obtain the velocity and altitude, the electron number density at each point in the trajectory is calculated using the method described above. Then, the power generated can be calculated for each point, giving a power vs. time curve that defines the amount of energy available for that trajectory. This curve is then ready for analysis by the electrical energy storage system model.

B. Electrical Energy Storage Systems

Electrical energy storage systems are extremely diverse in their mechanisms and applications. These systems can be mechanical, chemical, and electrodynamic in mechanism, while others still are combinations of these elements. Applications for electrical energy storage systems range from mobile devices to large water retention ponds capable of powering entire cities for long periods of time.[16] With such a diversity in mechanisms and applications, appropriate performance objectives upon which to evaluate electrical energy storage systems are challenging to develop. This problem is particularly troublesome for systems under development that may have an ill-defined application profile.

Examples of common electrical energy storage system performance parameters include mass, endurance, power capacity, longevity, and heat generation. The application being presently considered is a flight application, and thus mass is expected to play an extremely important role in the performance of such an energy storage system. In addition, although electrical energy storage system parameters such as longevity and heat generation are important, the assessment of their impact requires detailed system design information that is outside the scope of this analysis and typically not known without precise knowledge of the energy usage loads and flight system geometry. The total amount of electrical energy generated will allow for estimation of the size of energy storage device needed; however, as mentioned earlier the electrical energy generation for this application may occur at a relatively high rate that will place requirements on system power capacity as well.[16]

Thus, for the purposes of this analysis, total electrical energy storage system mass is determined to be the most important parameter. If some total amount of energy is to be generated at a certain rate, mass and energy requirements can be calculated. Both total energy storage capacity and discharge power capacity for an electrical energy storage system can be related to system mass by defining mass specific versions of each of these properties. Typical units are watt hours per kg and watts per kg for specific energy storage and power discharge capacity. Although electrical energy storage systems for a given type may vary in their values for the aforementioned parameters, there is typically

a range for each parameter that is considered appropriate for a given technology. These values are determined experimentally and continually evolve as new developments in energy storage techniques come to fruition. These ranges can be used to define a best, average, and worst case scenario for a given technology.

The electrical energy storage systems categories that will be considered in this analysis are batteries, capacitors, and miscellaneous devices such as flywheels and super conducting magnetic energy storage.

Batteries are used in a variety of both static and mobile situations, with applications ranging from low to high power. They involve some sort of chemical reaction that when activated generates electricity. Although the bulk system performance for a battery is a function of complex multi-step reactions in reality, the performance as measured by power and energy density can be abstracted to a rough function of mass. Batteries under consideration are chosen as being representative, though not exhaustive, of the rechargeable technologies available and listed in order of age include lead acid, nickel cadmium, and lithium ion. Each of these systems has a characteristic performance, proven robustness, and longevity that makes them representative of the category from a performance analysis perspective.

Capacitors are another electrical energy storage system type that has the potential for portability, but unlike batteries, they store their energy in an electrical field generated internally. They can thus be said to have an electrodynamic energy storage mechanism. Capacitors as typically seen in consumer electronics are electrolytic capacitors, consisting of two metal plates a certain distance apart filled with a dielectric. They can be made to withstand extremely high voltage and energy storage rates, but their specific total energy storage capacity is usually poor. Recently, new types of capacitors that do not involve conventional dielectrics, but instead achieve much higher capacitance through separation of charge along extremely short distances or electrochemical reactions. These capacitors, termed super or ultracapacitors, have energy charge and discharge rates comparable to conventional capacitors, but have much higher specific energy values. The performance ranges for both types are distinct, and together these ranges serve as useful characterizations for the technology.

Other electrical energy storage systems are considered in this analysis. Some of these systems are exotic in nature and are quite new. One example is superconducting magnetic energy storage. In this storage technique, the resistance-less property of a superconducting material is used to facilitate an extremely high loop current that results in a dense magnetic field. This magnetic field stores the electrical energy. Due to their superconductivity, such systems have very high power discharge and charge rates, and acceptable energy storage density. Disadvantages, however, include the cryogenics usually necessary to achieve superconductivity, the effect of the strong magnetic field on neighboring electronics, and overall system mass. Super conducting magnetic energy storage system performance may be enhanced by exploiting superconductivity of carbon nanotubes, reducing system weight while increasing specific energy and power capability.[17] Another type of electrical energy storage system considered is a flywheel based system, where electrical energy is stored mechanically, typically with the assistance of magnetic bearings. Such a system can store a relatively large amount of energy with minimal thermal loss and high discharge rates when needed. This system may also have additional effects on flight vehicles with regards to stability and control owing to the large rotating mass.

In summary, electrical energy storage systems performance can be represented as mass specific energy and discharge power capacity. For the present application of power generation and energy storage, charge power capacity and discharge power capacity are assumed to be roughly equal, simplifying the analysis. One way in which to visualize the performance of these systems is to plot the specific power vs. the specific energy storage capacity. Such a plot is termed a Ragone plot and is very useful for selecting power systems. For the application being considered, good choices generally lie to the top right of the chart, while poorer choices lie to the bottom left. A Ragone plot generated from industry data for the energy storage devices being considered is presented below as Figure 5.

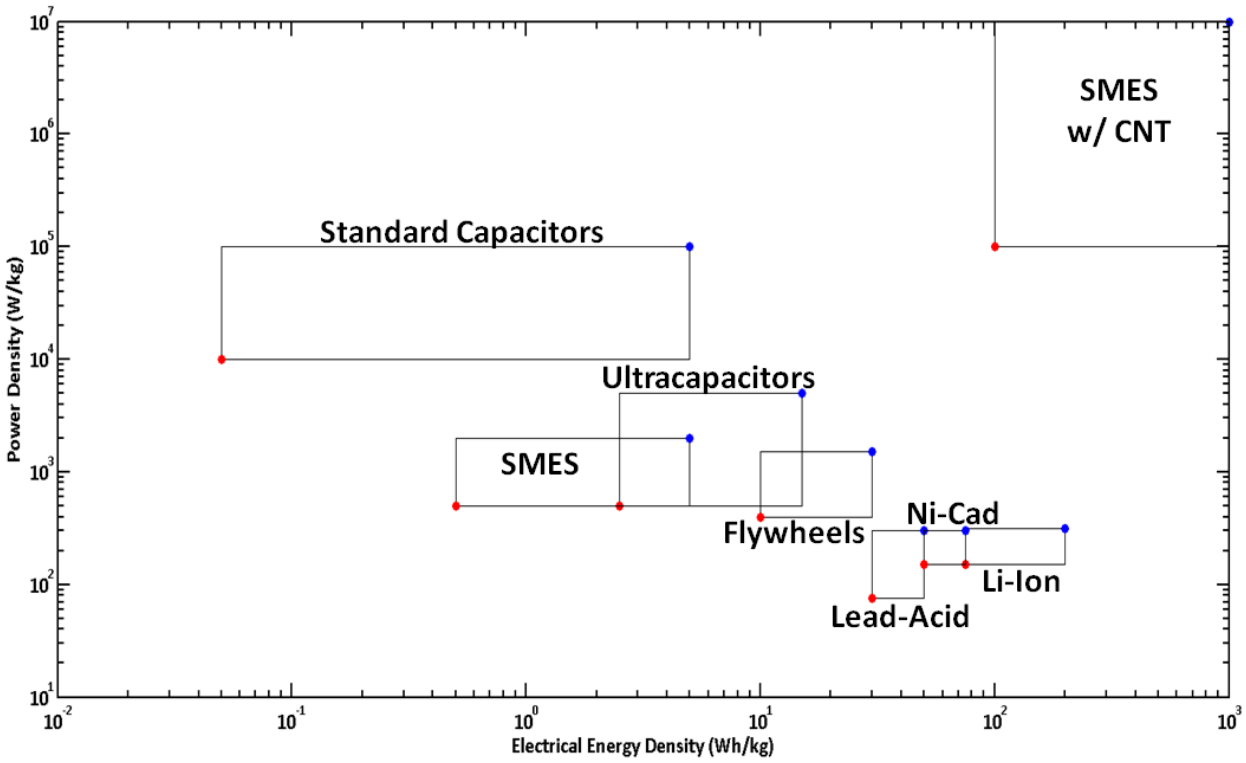

Figure 5. Ragone plot for electrical energy storage systems under consideration.

The plot presented above includes highlights of best and worst case scenarios, as represented by the red and blue dots respectively. These values do not necessarily represent any real device in particular, rather only the limits of a particular technology. Numerically, they are summarized along with an estimate of their technology readiness level (TRL) below in table 2.

Table 2 Electrical Energy Storage System Performance Data

EES System	Minimum Wh/kg	Maximum Wh/kg	Minimum W/kg	Maximum W/kg	Technology Readiness Level
Lead Acid	**30**	**50**	**75**	**300**	**High**
Nickel Cadmium	**50**	**75**	**150**	**300**	**High**
Lithium Ion	**75**	**200**	**150**	**315**	**High**
Capacitors	**0.05**	**5**	**10,000**	**100,000**	**Medium**
Ultracapacitors	**2.5**	**15**	**500**	**5,000**	**Medium**
SMES	**0.5**	**5**	**500**	**2,000**	**Low**
SMES w/ CNT	**100**	**1,000**	**100,000**	**10,000,000**	**Low**
Flywheels	**10**	**30**	**400**	**1,500**	**Low**

The values illustrated by this table give all necessary information to calculate the electrical energy storage system mass for a power vs. time profile for a given technology. In addition, it may prove useful to characterize electrical energy storage system performance by technology readiness level alone. This characterization is done by taking the best overall performer in each of the three TRL categories as representative of that category. The resulting average values for each TRL are presented below in table 3.

Table 3 Electrical Energy Storage System Performance Data

EES System TRL	Average Specific Energy (Wh/kg)	Average Specific Power (W/kg)
High (Lithium-Ion)	**137.5**	**232.5**
Medium(Ultracapacitors)	**8.75**	**2750**
Low (SMES w/ CNT)	**550**	**5,050,000**

III. Methodology and Experimental Design

A. Dynamical Model Implementation and Power Profile Construction

The aforementioned approach is implemented numerically in MATLAB. The temperature and pressure are written as simple functions of altitude based on relevant Mars atmospheric data, with temperature following a linear profile and pressure following an exponential one. The Martian atmospheric composition is known to be relatively constant with altitude[14] and in conjunction with the ideal gas law allows for the calculation of the density variation with altitude as well. The specification of the ambient temperature, pressure, composition, density completes all relevant Martian atmospheric inputs into the model.

Given initial conditions, the model calculates the position and velocity states as functions of time until the spacecraft's trajectory intersects with the Martian surface. In addition, the model is also set up to record and count each instance in which the spacecraft exits or leaves the Martian atmospheric boundary, taken in this case as an altitude of 100km. This tabulation is important in effectively determining the number of complete orbits made during a multi-pass entry trajectories as well as determining the total time spent in the atmosphere.

Table 4 Test Vehicle Configurations

Vehicle	Mass (kg)	C_D	A (m^2)	β (kg/m^2)
Mars Pathfinder	**582**	**1.68**	**5.52**	**63.1**
Mars Science Lab	**3151**	**1.68**	**16.6**	**112.9**
Moses Test Vehicle[4]	**1000**	**0.4**	**7.00**	**357.1**
Mars Human Mission	**100,000**	**1.68**	**78.5**	**757.9**

The test vehicle configurations considered in this analysis are presented above as Table 4 in order of increasing ballistic coefficient. For each configuration, the initial altitude and velocity was 100 km and 5 km/s respectively, and multi-pass entry trajectories were found experimentally by varying the initial flight path angle and solving the equations of motion to determine the number of passes and the total time in atmosphere. The result was a series of entry trajectories for each configuration, with number of passes ranging from two to ten. Here a 'pass' is defined as complete entry and exit of the atmosphere. Thus, a 10 pass case would enter and exit the atmosphere 10 times, followed by a final entry from which the spacecraft does not reemerge. An example plot of a 10 pass trajectory as generated by the model is given below as figure 6.

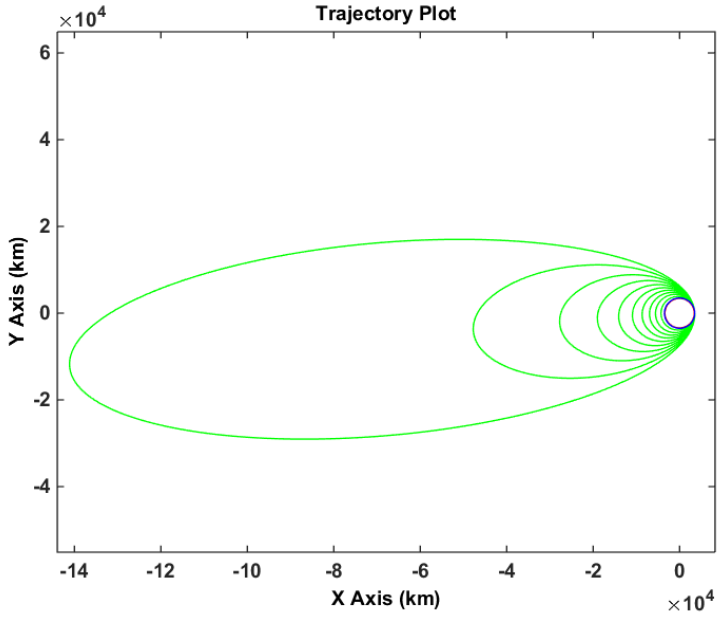

Figure 6. 10 pass trajectory view from above orbital plane.

The initial flight path angle and time in atmosphere for each multi-pass trajectory are summarized below in Table 4.

Table 5 Initial Conditions for Each Test Vehicle Configuration at 100 km Altitude and 5 km/s Velocity

Complete Passes	Mars Pathfinder		Mars Science Lab		Moses Test Vehicle		Mars Human Mission	
	$\gamma_{entry}(^o)$	Time in Atm(s)	$\gamma_{entry}(^o)$	Time in Atm(s)	$\gamma_{entry}(^o)$	Time in Atm(s)	$\gamma_{entry}(^o)$	Time in Atm(s)
2	-3.50	751	-4.20	1260	-5.50	1356	-6.35	1459
4	-2.05	1081	-3.05	1320	-4.65	2027	-5.65	2276
6	-1.40	1180	-2.35	1496	-4.05	2566	-5.20	2953
8	-1.00	1261	-1.75	1680	-3.60	2977	-4.80	3589
10	-0.85	1270	-1.45	1805	-3.20	3335	-4.50	4146

In addition, direct entry trajectories are also considered. For these trajectories, the initial velocity is set as 7 km/s to reflect typical interplanetary orbital velocities. However, to better facilitate comparison with the multi-pass trajectory cases, a 5 km/s direct entry case is also considered, having a velocity only 50 m/s higher than the Martian escape velocity. The initial flight path angle and time in the atmosphere for these trajectories are summarized in table 6 below.

Table 6. Initial Conditions for Each Test Vehicle Configuration at 100 km Altitude

Vehicle	7 km/s Entry Velocity		5 km/s Entry Velocity	
	$\gamma_{entry}(^o)$	Time in Atm(s)	$\gamma_{entry}(^o)$	Time in Atm(s)
Mars Pathfinder	-11.00	242	-11.00	240
Mars Science Lab	-11.00	223	-11.00	215
Moses Test Vehicle	-11.00	204	-11.00	175
Mars Human Mission	-11.00	215	-11.00	159

Each initial condition allows for computation of the position and velocity states throughout the corresponding trajectory, giving the altitude and speed at each point. The electron number density is calculated using NASA's CEA code to solve the post shock thermochemistry problem. Inputs are the freestream velocity, atmospheric composition, seed particle amount, and ambient atmospheric pressure and temperature. The atmospheric composition is as noted previously in table 1, and the seed particle mass fraction is varied up to 1% mass fraction potassium as indicated in previous studies.[4] The ambient pressure and temperature can be generalized as functions of altitude, such that the electron number density is essentially a function of altitude and velocity only. In order to expedite computation for

multiple runs, a lookup table for electron number density as a function of altitude and velocity is generated, with altitude varying from 0 to 100 km in 1km increments and velocity varying from 2500 – 7500 m/s in 100 m/s increments. These values cover the range of conditions and velocities suitable to MHD energy generation[4], with final electron number density linearly interpolated based on the table values.

B. Electrical Energy Storage System Performance Model

A model has been created that calculates the electrical energy storage system mass for a given power generation profile and energy storage system type. It does so by integrating the power generation vs. time profile curve to calculate the total energy available for storage while also noting the peak energy generation power. As shown in Figure 5 and table 2, both power and energy requirements define energy storage system mass. Thus, there are two possibilities, power capacity driven mass, and energy generation driven mass. Both approaches must be taken, and the final stored energy is assessed relative to the initial amount of energy. From the system mass and relative energy conversion metrics, an educated assessment can be made with regards to what energy storage system mass is most advantageous for a given technology.

The minimum and maximum pairs in Table 2 above define worst and best cases respectively. In addition, an average case can be generated. Thus, three distinct performance cases for each technology are selectable within the model by the user. The end result is to generate values for power and energy density given selections for energy storage system type and performance scenario. The process for doing so is described below as Figure 7.

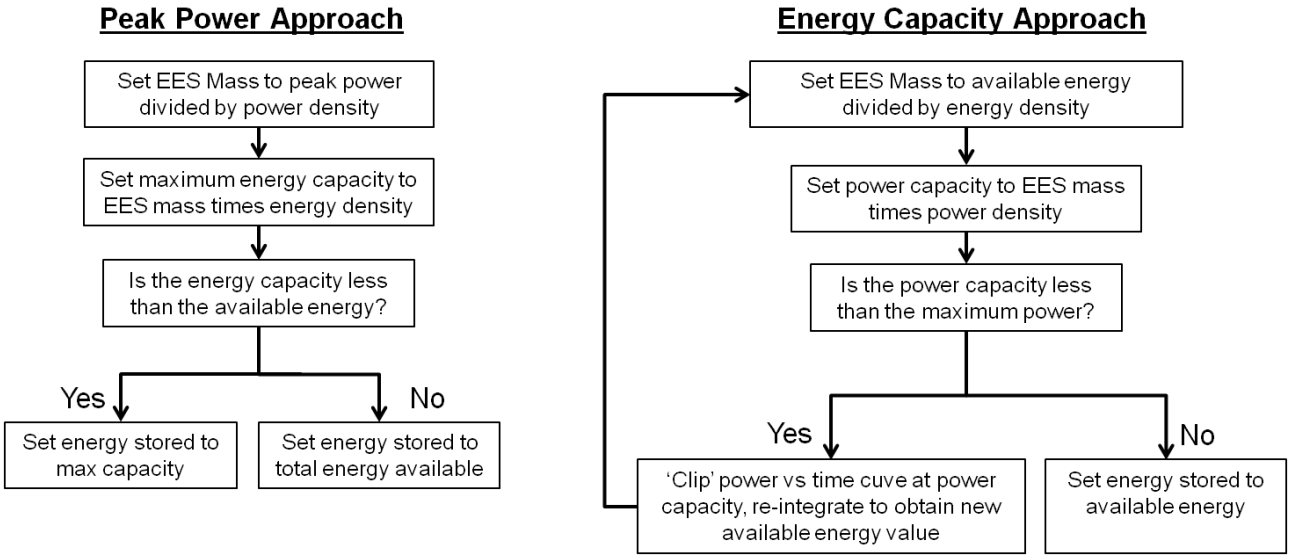

Figure 7. Electrical energy storage system model flowchart.

As shown in Figure 7, there are two approaches to finding energy storage system mass. The first approach, termed the 'Peak Power Approach', involves defining system power capacity as equal to the maximum energy generation rate from the given power profile. Dividing this system power capacity by the specific power capacity for the technology under consideration results in the system mass. Total stored energy is calculated by multiplying this mass by the specific energy capacity of the technology under consideration, and this value is compared with the total energy available. Depending on the technology, this approach may generate a very high or very low mass and very high or very low percent available energy stored.

The second approach, termed the 'Energy Capacity Approach', involves using the total available energy to drive system mass. An initial guess for the system mass is set by dividing total available energy by specific energy capacity for the technology in question. This initial guess for system mass is then used to calculate the power capacity of this system. If the power capacity is above the maximum power for the power profile, no further action is taken, otherwise, the power generation profile must be 'clipped' at the maximum power capacity rate for the system. Thus, a new power profile curve and associated total energy is generated, requiring that the initial guess for the mass be modified. This

process must be completed iteratively until a converged value for energy storage mass is found. At the completion of the process, the final mass determines the amount of energy stored, and it can be compared with the original amount of energy available from the power generation profile.

At the conclusion of this process, the model outputs the system mass and converted energy using both approaches in addition to the total energy available for conversion. Different technologies may result in one or the other approach being better than the other. For this analysis, the highest percent energy retained is chosen. Finally, there is an option to limit the total energy storage system mass to come predefined value, taken as 10% for this analysis.

A sample power generation profile for the Moses Entry Vehicle direct entry case from previous work is presented below as Figure 8.[4]

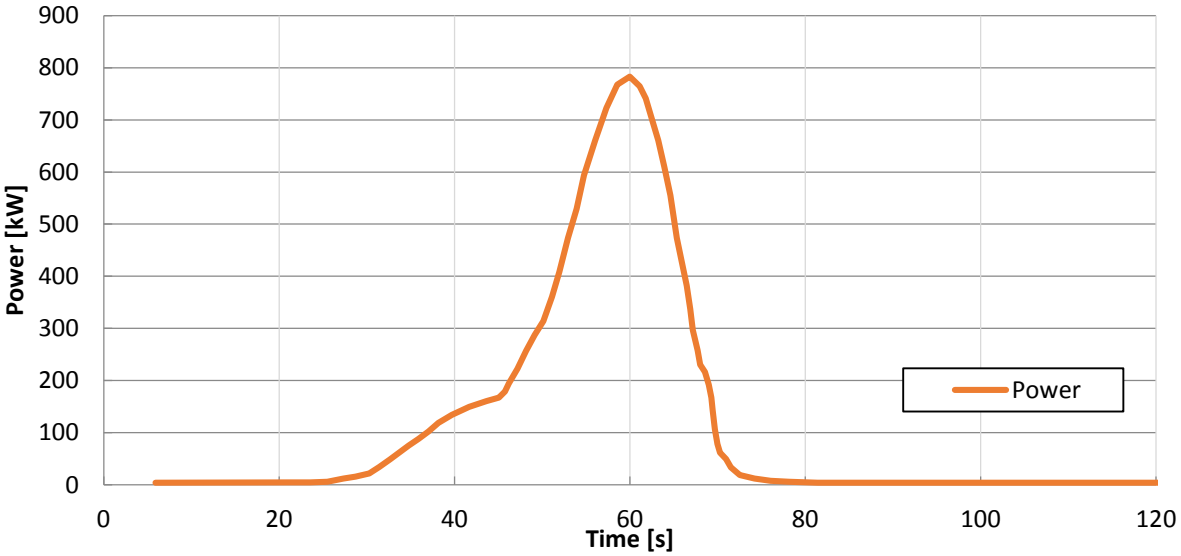

Figure 8. Direct entry power generation profile for Moses test vehicle.[4]

Analysis of the aforementioned power profile assuming no constraints on energy storage mass and average performance for each energy storage technology yields the mass data given in Table 7 below

Table 7 Moses Test Vehicle Direct Entry Electrical Energy Storage System Mass

EES Technology	Mass (kg)	Calculation Method
Li-Ion	3368	Peak Power
Lead Acid	4176	Peak Power
NiCad	3480	Peak Power
Capacitor	1551	Max Energy
Ultracapacitor	447.5	Max Energy
SMES	1424	Max Energy
SMES w/ CNT	7.120	Max Energy
Flywheel	824.2	Peak Power

Many of the energy storage system masses in Table 7 are above the original vehicle mass of 1000kg. In many cases, the mass is very high due to the limited power capacity in comparison to the energy capacity or vice versa. Since the energy storage system mass is a function of only two parameters, power density and energy density, a surface plot of the total energy stored while limiting mass to 10% of overall vehicle mass can be generated, given as Figure 9 below.

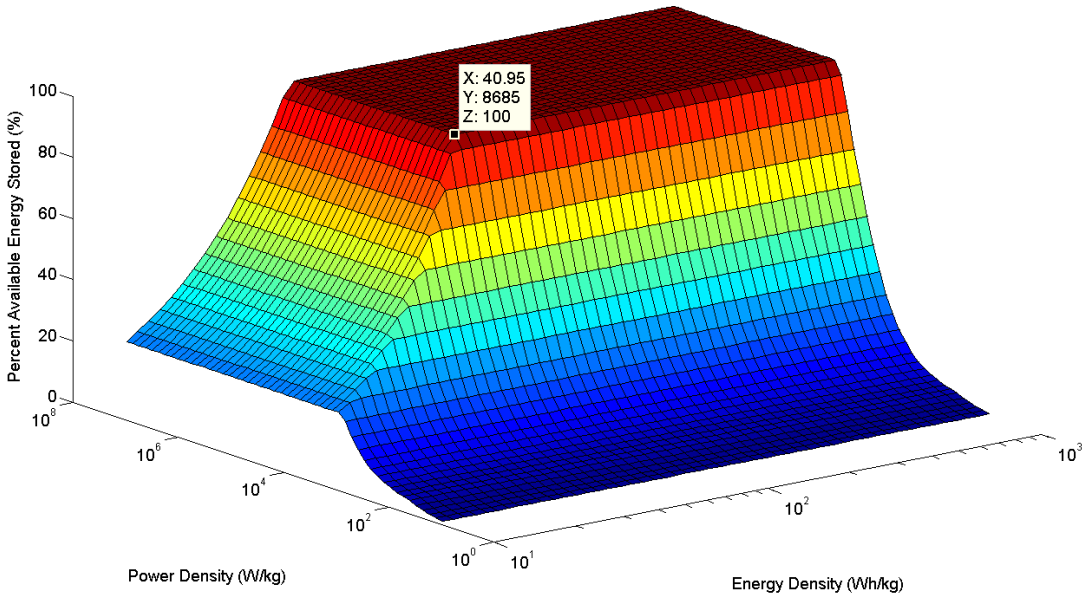

Figure 9. Percent available energy stored for Moses test vehicle direct entry case, mass constrained to 100kg.

As can be seen in Figure 9, the energy storage system is incapable of storing the available energy up to a certain point, marked with a data cursor. This point is of interest because it defines the minimum performance characteristics necessary for an energy storage system to satisfy a certain mass constraint and store all of the available energy without wasted storage capacity.

C. Parameter Study

Using the techniques and methodology discussed above, a parameter study was conducted. There existed a total of 5 possible potassium seeding mass fractions, 4 possible vehicle configurations, 7 possible trajectories, and 5 possible electrical energy storage system mass constraints. At each of the 700 possible sample points, the power available was calculated, and the total energy available and maximum power determined. Then, the performance of various electrical energy storage systems was assessed. The results of this study are presented in the following section, and the parameters are summarized as table 8.

Table 8 Parameter Study Names and Values

Seeding Levels	Vehicle Configurations	Trajectory Types	EES Mass Constraint
Unseeded	Mars Pathfinder	7km/s Direct	5% of Vehicle Mass
0.25% K Mass Fraction	Mars Science Lab	5km/s Direct	10% of Vehicle Mass
0.50% K Mass Fraction	Moses Test Vehicle	5km/s 2 Pass	15% of Vehicle Mass
0.75% K Mass Fraction	Mars Human Mission	5km/s 4 Pass	20% of Vehicle Mass
1.00% K Mass Fraction		5km/s 6 Pass	25% of Vehicle Mass
		5km/s 8 Pass	
		5km/s 10 Pass	

IV. Results and Discussion

In the following subsection, results are presented for the parameter study described by table 8. The performance of MHD energy generation during planetary entry is assessed by various metrics as a function of the parameters described by table 8.

A. Direct Entry Power vs Time Profiles at Various Seeding Levels

Power vs time profiles for the first two direct entry cases are presented below as Figures 10 – 19.

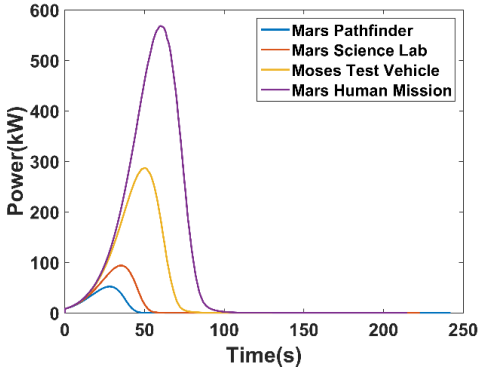

Figure 10. 7km/s Unseeded Power Profiles

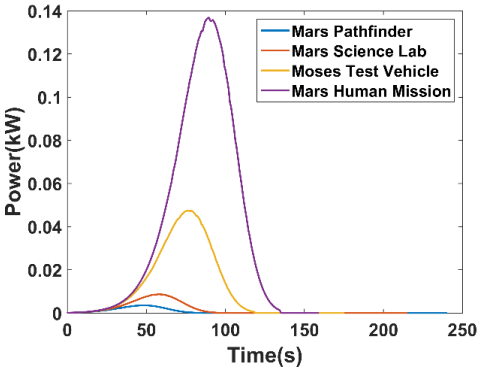

Figure 21. 5km/s Unseeded Power Profiles

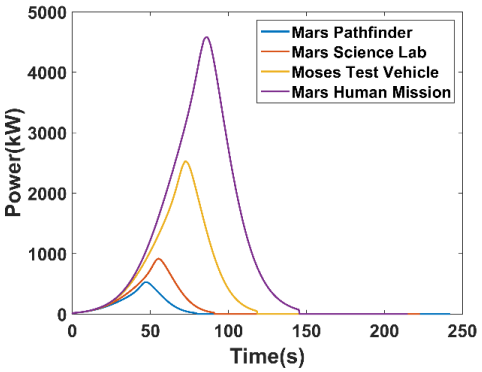

Figure 32. 7km/s 0.25% K Seeded Power Profiles

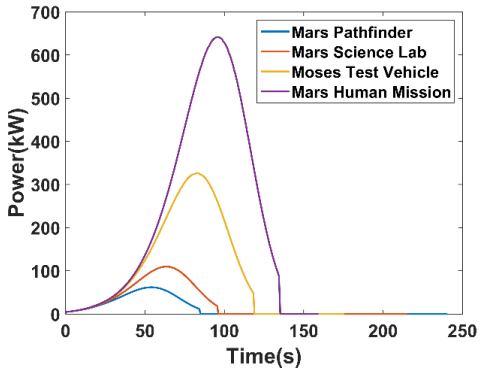

Figure 43. 5km/s 0.25% K Seeded Power Profiles

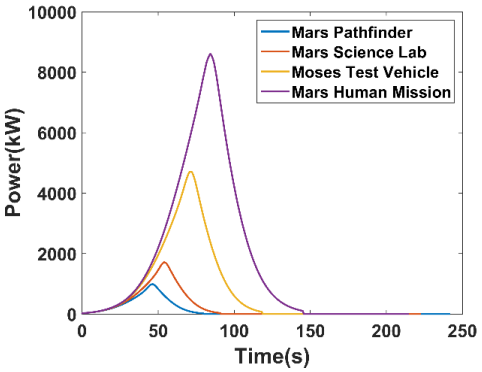

Figure 54. 7km/s 0.50% K Seeded Power Profiles

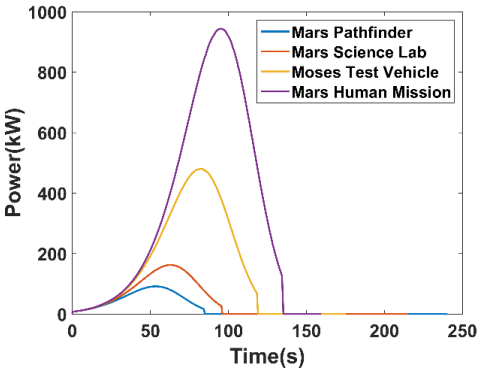

Figure 65. 5km/s 0.50% K Seeded Power Profiles

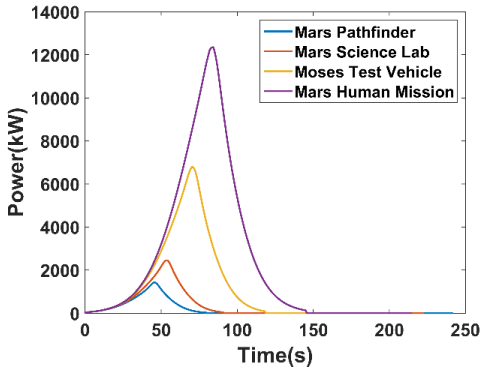

Figure 76. 7km/s 0.75% K Seeded Power Profiles

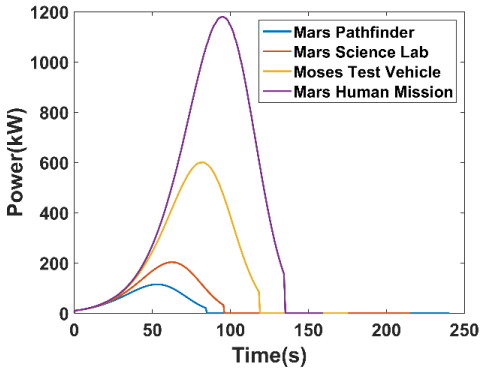

Figure 87. 5km/s 0.75% K Seeded Power Profiles

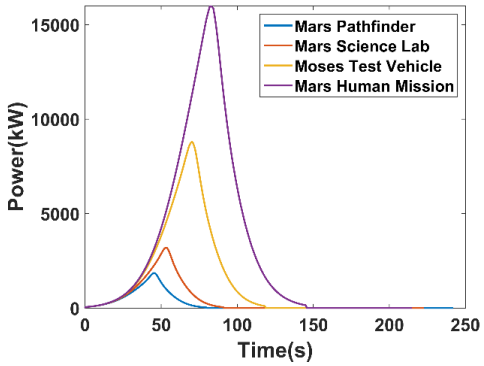

Figure 98. 7km/s 1.00% K Seeded Power Profiles

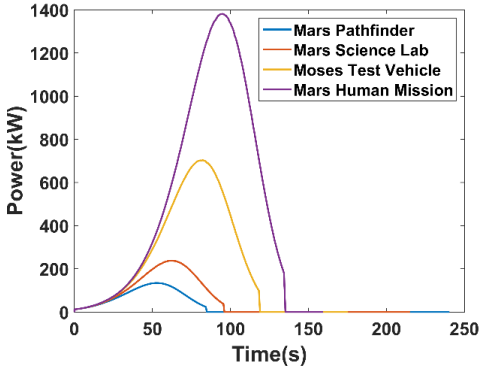

Figure 109. 5km/s 1.0% K Seeded Power Profiles

The exceptionally strong dependence of post shock electron number density on velocity in the unseeded Martian atmosphere is apparent in the low power level shown in Figure 11 above. Although there are similar functional forms between the 7km/s and 5km/s direct entry cases, the power levels are drastically different, often differing by up to one order of magnitude or more. From Figures 10 – 19 it is also apparent that the amount of power available for MHD energy generation goes up with increasing ballistic coefficients. This is to be expected due to the strong velocity dependence of the post shock electron number density illustrated in Figure 4. Moreover, vehicles with high ballistic coefficients tend to decelerate lower in the atmosphere, not only maintaining higher velocities for longer periods of time, but also maintaining those relatively higher velocities at lower altitudes with higher free stream densities. Figures 2, 3, and 4 confirm the dependence of post shock electron number density on altitude as well. The results for the total available energy for the 7km/s entry cases are presented below in table 9. Energy availability and peak power for the 5km/s direct entry cases are presented in the subsequent subsection.

Table 9. 7 km/s Direct Entry Total Available Energy and Peak Power for all Vehicle Cases and Seed Levels

Vehicle	Mars Pathfinder		Mars Science Lab		Moses Test Vehicle		Mars Human Mission	
Potassium Seeding Level	Total Energy Available (MJ/m^2)	Peak Power (kW/m^2)	Total Energy Available (MJ/m^2)	Peak Power (kW/m^2)	Total Energy Available (MJ/m^2)	Peak Power (kW/m^2)	Total Energy Available (MJ/m^2)	Peak Power (kW/m^2)
Unseeded	1.36	52.24	2.65	93.77	9.44	287.26	20.93	568.30
0.25%	15.54	528.44	29.04	916.98	96.94	2524.83	209.12	4585.37
0.50%	27.48	987.19	51.35	1711.76	171.16	4709.60	368.68	8614.05
0.75%	38.63	1428.22	72.19	2476.71	240.45	6792.40	517.43	12359.46
1.0%	49.29	1853.51	92.13	3205.28	306.64	8803.19	659.30	15989.27
$R_{1\%/Unseeded}$	36.22	35.48	34.71	34.18	32.48	30.65	31.50	28.14

B. 5km/s Trajectory Power Profile Summaries at Each Seeding Level

In addition to the direct entry cases illustrated in Figures 10 – 19, power profiles were computed at all 5km/s trajectories, denoted by trajectory cases 2 – 7. These cases correspond to an entry after a propulsive orbit insertion or aerocapture event. The 5km/s direct entry case is included to facilitate comparison with the multi-pass trajectories, which consist of several aerobraking orbital passes followed by an entry from orbit. The total available energy and peak power rate for these trajectories are presented for all vehicles and seeding levels as tables 10 – 14 below.

Table 10. Unseeded Total Available Energy and Peak Power for all Vehicle Cases

Vehicle	Mars Pathfinder		Mars Science Lab		Moses Test Vehicle		Mars Human Mission	
Number of Passes	Total Energy Available (MJ/m^2)	Peak Power (kW/m^2)	Total Energy Available (MJ/m^2)	Peak Power (kW/m^2)	Total Energy Available (MJ/m^2)	Peak Power (kW/m^2)	Total Energy Available (MJ/m^2)	Peak Power (kW/m^2)
Direct	0.00	0.00	0.00	0.01	0.00	0.05	0.01	0.14
2	0.00	0.00	0.00	0.00	0.00	0.00	0.00	0.01
4	0.00	0.00	0.00	0.00	0.00	0.00	0.00	0.01
6	0.00	0.00	0.00	0.00	0.00	0.00	0.00	0.00
8	0.00	0.00	0.00	0.00	0.00	0.00	0.00	0.00
10	0.00	0.00	0.00	0.00	0.00	0.00	0.00	0.00
$R_{direct/10Pass}$	N/A	N/A	N/A	N/A	N/A	N/A	N/A	N/A

Table 11. 0.25% K Seeded Total Available Energy and Peak Power for all Vehicle Cases

Vehicle	Mars Pathfinder		Mars Science Lab		Moses Test Vehicle		Mars Human Mission	
Number of Passes	Total Energy Available (MJ/m^2)	Peak Power (kW/m^2)	Total Energy Available (MJ/m^2)	Peak Power (kW/m^2)	Total Energy Available (MJ/m^2)	Peak Power (kW/m^2)	Total Energy Available (MJ/m^2)	Peak Power (kW/m^2)
Direct	2.89	62.00	5.34	109.85	17.15	326.01	35.78	641.49
2	2.00	9.21	4.01	15.49	15.59	45.92	35.76	103.19
4	1.51	5.66	3.28	8.78	13.99	25.72	33.72	58.92
6	1.35	5.01	2.87	6.70	12.72	17.60	32.03	41.52
8	1.28	4.81	2.58	5.63	11.69	13.39	30.42	30.87
10	1.26	4.77	2.47	5.28	10.83	10.75	29.10	25.01
$R_{direct/10Pass}$	1.59	1.93	1.63	2.94	1.44	4.27	1.23	4.13

Table 12. 0.50% K Seeded Total Available Energy and Peak Power for all Vehicle Cases

Vehicle	Mars Pathfinder		Mars Science Lab		Moses Test Vehicle		Mars Human Mission	
Number of Passes	Total Energy Available (MJ/m^2)	Peak Power (kW/m^2)	Total Energy Available (MJ/m^2)	Peak Power (kW/m^2)	Total Energy Available (MJ/m^2)	Peak Power (kW/m^2)	Total Energy Available (MJ/m^2)	Peak Power (kW/m^2)
Direct	4.32	91.60	7.96	162.33	25.50	480.66	53.11	944.41
2	3.01	14.21	6.04	23.88	23.38	70.62	53.46	157.90
4	2.28	8.93	4.95	13.75	21.03	40.08	50.53	91.31
6	2.05	7.98	4.33	10.58	19.13	27.64	48.07	64.76
8	1.93	7.70	3.90	8.95	17.60	21.13	45.70	48.39
10	1.90	7.66	3.73	8.41	16.32	17.02	43.74	39.34
$R_{direct/10Pass}$	1.58	1.86	1.62	2.84	1.43	4.15	1.22	4.01

Table 13. 0.75% K Seeded Total Available Energy and Peak Power for all Vehicle Cases

Vehicle	Mars Pathfinder		Mars Science Lab		Moses Test Vehicle		Mars Human Mission	
Number of Passes	Total Energy Available (MJ/m^2)	Peak Power (kW/m^2)	Total Energy Available (MJ/m^2)	Peak Power (kW/m^2)	Total Energy Available (MJ/m^2)	Peak Power (kW/m^2)	Total Energy Available (MJ/m^2)	Peak Power (kW/m^2)
Direct	5.43	114.65	10.01	203.13	32.02	600.92	66.62	1180.17
2	3.80	18.14	7.62	30.47	29.45	89.98	67.27	200.82
4	2.88	11.52	6.26	17.68	26.52	51.39	63.64	116.76
6	2.59	10.34	5.47	13.65	24.14	35.56	60.58	83.07
8	2.45	10.01	4.94	11.58	22.21	27.26	57.62	62.23
10	2.41	9.96	4.71	10.90	20.60	21.99	55.17	50.67
$R_{direct/10Pass}$	1.58	1.82	1.62	2.79	1.43	4.09	1.22	3.96

Table 14. 1.00% K Seeded Total Available Energy and Peak Power for all Vehicle Cases

Vehicle	Mars Pathfinder		Mars Science Lab		Moses Test Vehicle		Mars Human Mission	
Number of Passes	Total Energy Available (MJ/m^2)	Peak Power (kW/m^2)	Total Energy Available (MJ/m^2)	Peak Power (kW/m^2)	Total Energy Available (MJ/m^2)	Peak Power (kW/m^2)	Total Energy Available (MJ/m^2)	Peak Power (kW/m^2)
Direct	6.38	134.41	11.76	237.95	37.59	703.54	78.17	1381.41
2	4.47	21.50	8.97	36.11	34.64	106.57	79.07	237.58
4	3.39	13.74	7.37	21.05	31.21	61.10	74.85	138.61
6	3.06	12.38	6.45	16.30	28.42	42.36	71.27	98.80
8	2.89	12.00	5.82	13.86	26.16	32.52	67.81	74.12
10	2.84	11.94	5.56	13.05	24.27	26.27	64.93	60.41
$R_{direct/10Pass}$	1.57	1.80	1.61	2.77	1.43	4.06	1.22	3.93

Table 10 makes it immediately apparent that seeding is necessary to generate any power for 5km/s entry velocities, regardless of trajectory type. The direct entry case does the best of all of these, but differs from the seeded cases in tables 11 through 14 by multiple orders of magnitude. Within tables 11 through 14, a trend can be observed in that both the total amount of available energy and peak power decrease with increasing number of passes through the atmosphere; however, peak power usually decreases by a larger margin than the total energy available. This difference is more noticeable for the higher ballistic coefficient Moses Test Vehicle and Mars Human Mission vehicle cases. For example, in the 1.00% K seeded case, where the total energies and peak power levels are highest, there a 10 pass orbit makes sense for the Human mission or Moses Test Vehicle, due to the ~1.5 factor decrease in available energy in exchange for a ~4 factor decrease of the peak power level. Lower peak power levels, as shown by figure 5 above, tend to correlate well with the capabilities of high energy density existing energy storage technologies such as lithium-ion batteries. For the lower ballistic coefficient Mars Pathfinder and Mars Science Lab, there is not as much benefit to be had by employing multi-pass entry trajectories due to the ~1.5 factor decrease in total energy in exchange for ~2-2.5 factor decrease in peak power rate.

C. 5km/s Entry Cases Electrical Energy Storage System Performance as a Function of Mass Constraint

At each point of the parameter search, an assessment of the energy storage system performance as characterized by amount of energy stored under a given mass constraint was made. Energy storage system parameter considered were the High, Medium, and Low TRL representative energy storage systems whose parameters were given in table 3. Figures 20-31 depict the effect of mass constraint applied to the three representative energy storage systems for all four vehicle cases at 1% K seeding level, as that had the most amount of energy available of the 5km/s entry cases.

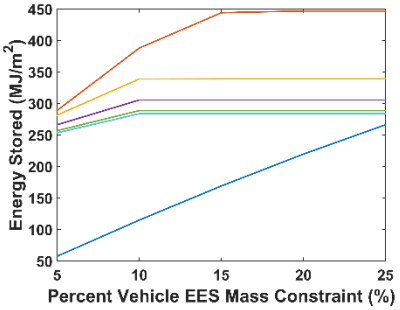

Figure 20. MPF High TRL EES Performance

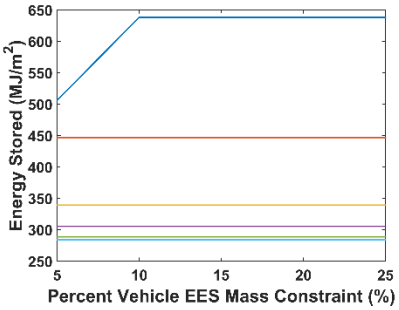

Figure 21. MPF Medium TRL EES Performance

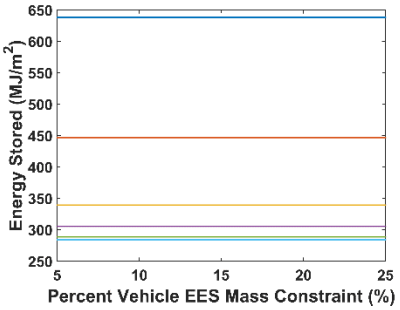

Figure 22. MPF Low TRL EES Performance

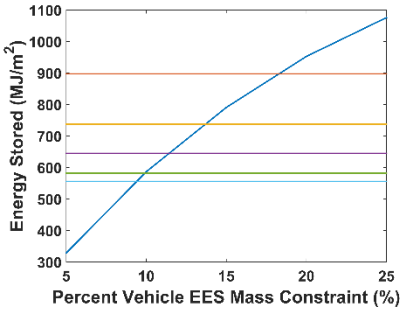

Figure 23. MSL High TRL EES Performance

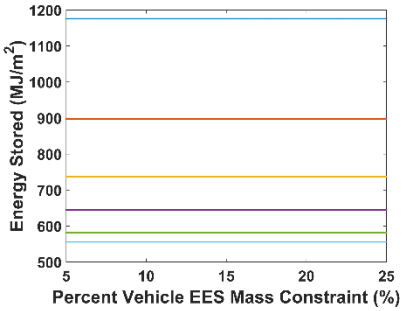

Figure 24. MSL Medium TRL EES Performance

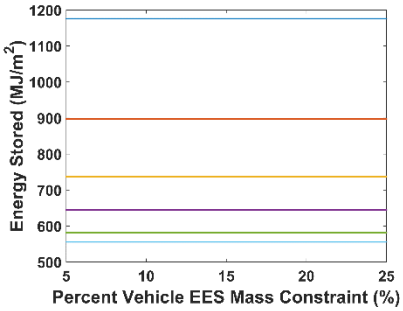

Figure 25. MSL Low TRL EES Performance

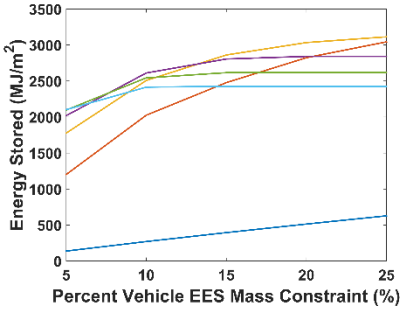

Figure 26. MOSES High TRL EES Performance

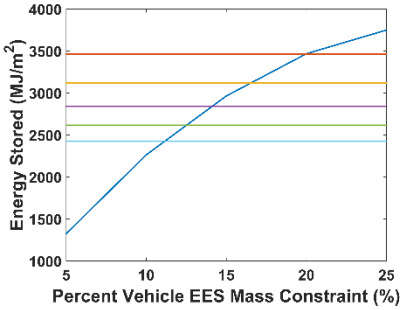

Figure 27. MOSES Medium TRL EES Performance

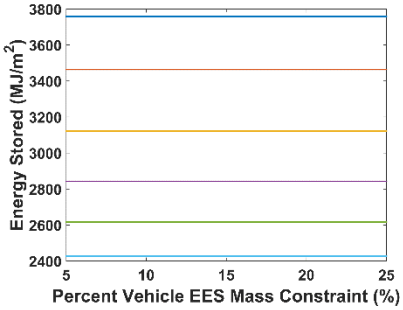

Figure 28. MOSES Low TRL EES Performance

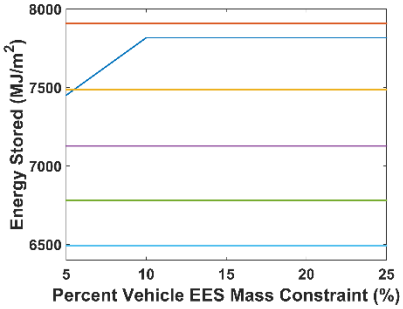

Figure 29. HUMAN High TRL EES Performance

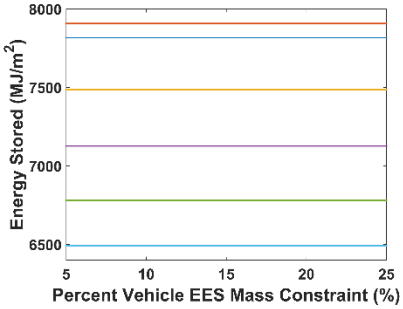

Figure 30. HUMAN Medium TRL EES Performance

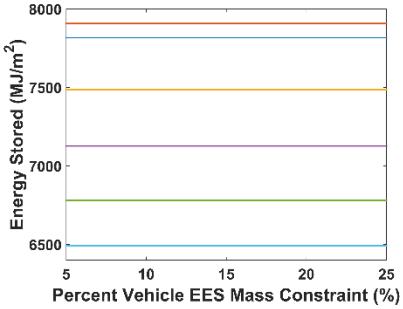

Figure 31. HUMAN Low TRL EES Performance

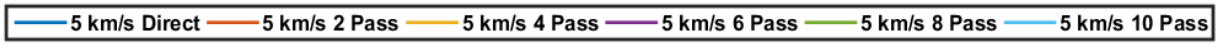

The results above show some slight constraining of the energy storage level for the 5km/s direct entry trajectory with decreasing mass allocation, confined to the high and medium technology readiness levels. Thus for typical Mars

robotic exploration entry vehicles, high TRL energy storage technologies are limited not by the available power for MHD energy generation, but rather by their capabilities to store the available energy. The more massive the entry vehicle initially, the higher the mass constraint and the lower the demands on the performance of the energy storage system, as illustrated by the Mars Human Mission in Figure 29. In fact, for the Human class mission, none of the 5km/s trajectories were limited by energy storage system performance at medium and high TRLs. These results indicate that more massive future Human missions to Mars may be able to store the energy from MHD energy generation within a reasonable mass envelope.

It may be useful to have an idea of how much energy storage system performance is being constrained by mass for the 5km/s direct entry cases. The unconstrained energy storage masses required to store all available energy for the 5km/s direct entry with 1% K seeding is presented below as table 15.

Table 15. 1% K Seeded 5km/s Direct Entry Unconstrained Energy Storage Mass Estimates

Vehicle	Mars Pathfinder	Mars Science Lab	Moses Test Vehicle	Mars Human Mission
EES Name	**EES Mass(kg)**	**EES Mass(kg)**	**EES Mass(kg)**	**EES Mass(kg)**
Lithium-Ion	**578.1**	**1023.4**	**3026.0**	**5941.6**
Lead Acid	**716.9**	**1269.1**	**3752.2**	**7367.5**
NiCad	**597.4**	**1057.6**	**3126.8**	**6139.6**
Capacitor	**702.3**	**1293.5**	**4135.2**	**8599.6**
Ultracapacitor	**202.7**	**373.3**	**1193.3**	**2481.6**
SMES	**644.9**	**1187.7**	**3796.8**	**7896.0**
SMES CNT	**3.2**	**5.9**	**19.0**	**39.5**
Flywheel	**141.5**	**250.5**	**740.6**	**1454.1**

As is shown in table 15 above, some of the energy storage technologies are poor choices for MHD energy generation during entry, with required masses well in excess of the entire entry vehicle under consideration. However, some emerging energy storage technologies such as SMES w/ CNT could prove very promising for flight applications. These results indicate much opportunity for improvement in energy storage system performance; however the importance of energy storage system performance is also dependent on the mass allocation by the mission in question.

D. 7km/s Direct Entry

As was shown in table 9, the total energy generated can be very large for the 7km/s direct entry cases, which is more representative of true interplanetary trajectory velocity at Mars. In addition, this energy is generated with high peak power rates, possibly resulting in more demands on the energy storage system and scaling with mass constraint. Plots similar to those shown in Figures 20 – 31 are given below as figures 32-43, this time encompassing all of the possible seeding values.

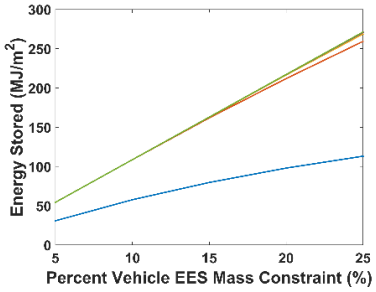

Figure 32. MPF High TRL EES Performance

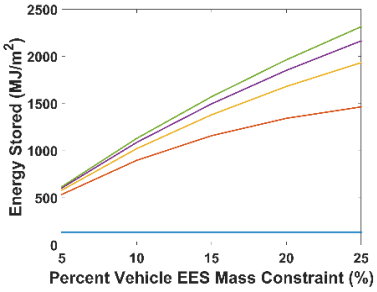

Figure 33. MPF Medium TRL EES Performance

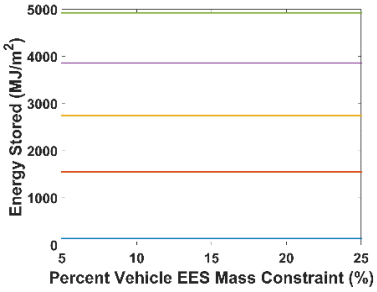

Figure 34. MPF Low TRL EES Performance

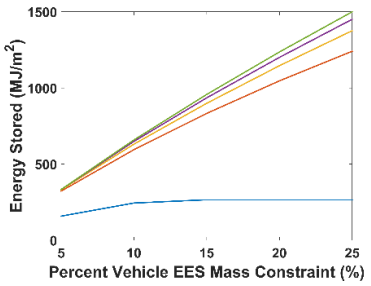

Figure 35. MSL High TRL EES Performance

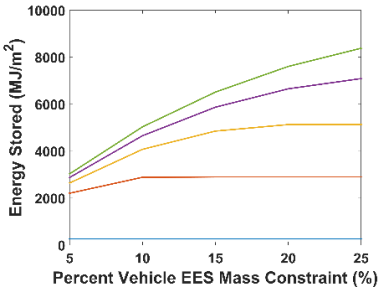

Figure 36. MSL Medium TRL EES Performance

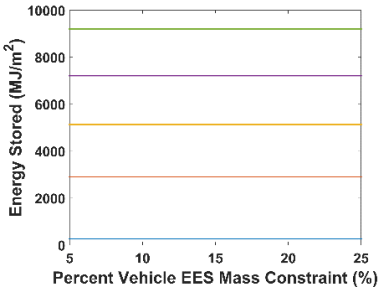

Figure 37. MSL Low TRL EES Performance

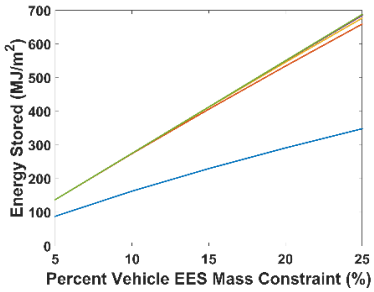

Figure 38. MOSES High TRL EES Performance

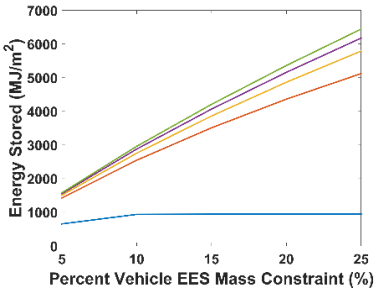

Figure 39. MOSES Medium TRL EES Performance

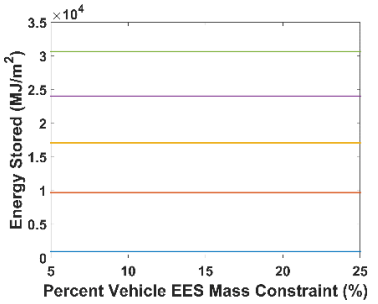

Figure 40. MOSES Low TRL EES Performance

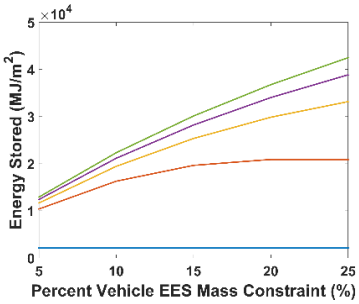

Figure 41 HUMAN High TRL EES Performance

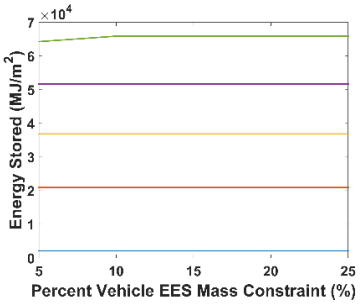

Figure 42 HUMAN Medium TRL EES Performance

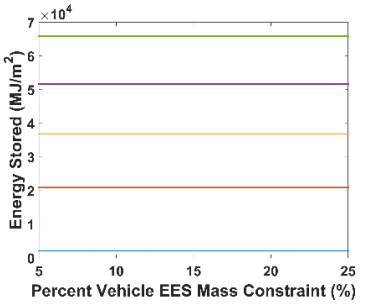

Figure 43 HUMAN Low TRL EES Performance

The results above show a fairly strong dependence on overall mass constraint at High and Medium TRLs for all but the Mars Human Mission. It is hypothesized that this dependence comes about due to the high power levels inherent in direct entry and the relatively low specific power of high TRL battery technology. However, if Medium or Low TRL energy storage systems are employed, the dependence on mass constraint is reduced or eliminated. These results indicate strong dependence on further technology development for electrical energy storage systems. Currently, only the Mars Human Class mission is unhampered by mass constraint with the Medium TRL energy storage systems, with other missions basically requiring low TRL energy storage systems. Thus, it seems most realistic to store all of the available energy on a future Mars Human Class mission.

Similar to the previous subsection, the unconstrained energy storage values can be computed for the 7km/s direct entry cases. The results are given below as table 16.

Table 16. 1% K Seeded 7km/s Direct Entry Unconstrained Energy Storage Mass Estimates

Vehicle	Mars Pathfinder	Mars Science Lab	Moses Test Vehicle	Mars Human Mission
EES Name	**EES Mass(kg)**	**EES Mass(kg)**	**EES Mass(kg)**	**EES Mass(kg)**
Lithium-Ion	**7972.1**	**13786.1**	**37863.2**	**68771.1**
Lead Acid	**9885.4**	**17094.8**	**46950.3**	**85276.1**
NiCad	**8237.8**	**14245.7**	**39125.3**	**71063.4**
Capacitor	**5422.9**	**10135.0**	**33734.1**	**72529.9**
Ultracapacitor	**1564.9**	**2924.7**	**9734.7**	**20930.1**
SMES	**4979.2**	**9305.8**	**30974.0**	**66595.7**
SMES CNT	**24.9**	**46.5**	**154.9**	**333.0**
Flywheel	**1951.1**	**3374.0**	**9266.5**	**16830.8**

The results shown in table 16 are indicative of current energy storage technologies being inadequate to meet the volume of energy that can be obtained via MHD energy generation for 7km/s direct entry. In fact, the only energy storage technology that is less than the 10 percent of the original mass of the entry vehicle in each case is the SMES w/ CNT, a low TRL energy storage system. Thus if complete storage of the energy from a 1 m^2 MHD generator is to be made, then the only option is to further develop energy storage technology.

E. Minimum Energy Storage System Performance Required to Store 100% of Available Energy

For all the trajectory cases at the highest seeding level of 1% and the lowest mass constraint of 5% entry mass, the minimum required energy storage system performance to store 100% of the available energy is presented. These cases represent the most extreme demands on the energy storage system and are thus a good indicator of the cases in which energy stored is limited by energy storage system performance. The results are presented as table 17 below.

Table 17. Minimum EES System Performance at 1% K Seeding and 5% Entry Mass Constraint

Vehicle	Mars Pathfinder		Mars Science Lab		Moses Test Vehicle		Mars Human Mission	
Trajectory	Min Specific Energy (Wh/kg)	Min Specific Power (W/kg)	Min Specific Energy (Wh/kg)	Min Specific Power (W/kg)	Min Specific Energy (Wh/kg)	Min Specific Power (W/kg)	Min Specific Energy (Wh/kg)	Min Specific Power (W/kg)
7 km/s Direct	**498**	**70548**	**163**	**23101**	**1831**	**187382**	**37**	**3275**
5 km/s Direct	**64**	**4977**	**21**	**1630**	**215**	**15199**	**<10**	**305**
5 km/s 2 Pass	**44**	**811**	**16**	**231**	**196**	**2154**	**<10**	**<100**
5 km/s 4 Pass	**34**	**534**	**13**	**152**	**179**	**1233**	**<10**	**<100**
5 km/s 6 Pass	**31**	**464**	**12**	**115**	**163**	**933**	**<10**	**<100**
5 km/s 8 Pass	**28**	**464**	**11**	**<100**	**148**	**705**	**<10**	**<100**
5 km/s 10 Pass	**28**	**464**	**<10**	**<100**	**135**	**534**	**<10**	**<100**

As can be seen in table 17 above, the minimum energy storage system performance requirements in general go down with increasing system mass, except in the case of minimum specific power for the Moses test vehicle, owing to its high ballistic coefficient and low mass. For the direct entry cases, the minimum specific powers are much higher than the minimum specific powers for the multi-pass cases, while the minimum specific energies are comparable provided that the same entry velocity is used. These numbers indicate that the specific power of the energy storage system is the primary limiting factor for energy storage for the direct entry case, followed by total mass constraint available for electrical energy storage.

V. Summary, Conclusions, and Future Work

An analysis capability for MHD generator equipped entry descent and landing systems has been developed. This capability includes a trajectory model, Martian atmospheric model, and post shock chemical equilibrium code implementation. In addition, several configurations were examined to study the trade between configurations, multi-pass orbits, and energy storage system technologies. It was generally found that increased ballistic coefficients resulted in higher available energy per meter squared of generator energy and that multi-pass orbits tended to reduce the power requirements dramatically while having a moderate decrease in total available energy provided there was sufficient seeding. Direct entries, particularly at higher velocities with seed particle are attractive options as well, but high power levels pose challenges for current energy storage technologies.

Future work includes extension of the model with a finite rate chemistry model and magnetohydrodynamic flow code as well as examination of the possibility of MHD flow control for hypersonic aero-maneuvering. This work will involve development of a custom computational fluid dynamics, chemistry, and magnetohydrodynamic code for the Martian atmosphere, as well as iteration on the nominal vehicle trajectory to assess the effect of the Lorentz forces acting on the vehicle.

Acknowledgments

This work is funded through a NASA Space Technology Research Fellowship, grant number NNX13AL82H. In addition, the authors would like to thank Dr. Robert Moses of NASA Langley research center for their advice towards the completion of this work.

References

[1]Braun, R.D., Manning, R.M., *Mars Exploration Entry, Descent and Landing Challenges*, IEEE Aerospace Conference, 4-11 March 2006.

[2]Spencer, D., Blanchard, R., Braun, R., *Pathfinder Entry, Descent, and Landing Reconstruction*, AIAA Journal of Rockets, Vol. 36, No. 3, May-June 1999.

[3] Jarvinen, P.O., *On the Use of Magnetohydrodynamics During High Speed Re-Entry*, AIAA Journal of Rockets, Avco-Everett Research Laboratory, Research Note 463, July 1964.

[4]Moses, R.W., Kuhl, CA., and Templeton, J.D., *Plasma Assisted ISRU at Mars*, 15th International conference on MHD Energy Conversion, Moscow, Russia, 24-27 May 2005.

[5]Macheret, S.O., Shneider, M.N., Candler, G.V., Moses, R.W., and Kline, J.F., *Magnetohydrodynamic Power Generation for Planetary Entry Vehicles*, 35th AIAA Plasmadynamics and Lasers Conference, Portland, Oregon, 28 June – 1 July 2004.

[6]Vuskovic, L., Popovic, S., Drake, J., and Moses, R.W., *Magnetohydrodynamic Power Generation in the Laboratory Simulated Martian Entry Plasma*, 15th International conference on MHD Energy Conversion, Moscow, Russia, 24-27 May 2005.

[7]Popovic, S., Moses, R.W., and Vuskovic, L., *System Development for Mars Entry In Situ Resource Utilization*, 8th Interplanetary Probe Workshop, Portsmouth, VA, 6-10 June 2011.

[8]Sparacino, et. al, *Survey of Battery Energy Storage Systems and Modeling Techniques*, IEEE Power and Energy Society General Meeting,San Diego, California, 22-26 July 2012.

[9]Repic, E.M., Boobar, M.G., and Chapel F.G., *Aerobraking as a Potential Planetary Capture Mode*, AIAA Journal of Spacecraft, Vol. 5, No. 8, August 1968.

[10]Johnston, et. al, *Mars Global Surveyor Aerobraking at Mars*, AAS/AIAA Space Flight Mechanics Meeting, Monterey, California, 9-11 February 1998.

[11]Smith, J. C. and Bell, J. L., *2001 Mars Odyssey Aerobraking*, AIAA Journal of Spacecraft and Rockets, Vol. 42, No 3, May–June 2005.

[12]Lyons, D. T., *Mars Reconnaissance Orbiter: Aerobraking Trajectory*, AIAA/AAS Astrodynamics Specialist Conference and Exhibit, Monterey, California, 5-8 August 2002.

[13]S. Gordon and B. J. McBride, "*Computer Program for Calculation of Complex Chemical Equilibrium Compositions and Applications*," NASA Reference Publication 1311, 1996.

[14]Mahaffy et al., "*Abundance and Isotopic Composition of Gases in the Martian Atmosphere from the Curiosity Rover*," Science, Vol. 341, No. 6143, page 263-266, July 2013.

[15]Candler, G., "*Computation of Thermo-Chemical Nonequilibrium Martian Atmospheric Entry Flows*," AIAA/ASME 5th Joint Thermophysics and Heat Transfer Conference, Seattle, WA, June 18-20, 1990.

[16]Chen, H., et. al, *Progress in Electrical Energy Storage System: A Critical Review*, Progress in Natural Science, Vol. 19, Issue 3, pages 291 - 312, 10 March 2009.

[17]LyTec, LLC, *Flight-Weight Magnets Using Carbon Nanotubes*, LyTec-R-02-012, 2 May 2002.

[18]Ribeiro, et. al., *Energy Storage Systems for Advanced Power Applications*, IEEE, Vol. 89, No. 12, page 1745, December 2001.